Title
Modeling of a Growing Oxide Film: The Iron/Iron Oxide System

Journal
Journal of the Electrochemical Society, 142(5)

Authors
Battaglia, V.
Newman, J.

Publication Date
1993-07-20

LBL-34385
UC-213
Preprint

Lawrence Berkeley Laboratory
UNIVERSITY OF CALIFORNIA

Materials Sciences Division

Submitted to Journal of the Electrochemical Society

Modeling of a Growing Oxide Film: The Iron/Iron Oxide System

V. Battaglia and J. Newman

July 1993

Prepared for the U.S. Department of Energy under Contract Number DE-AC03-76SF00098

DISCLAIMER

LBL-34385
UC-213

Modeling of a Growing Oxide Film: The Iron/Iron Oxide System

Vincent Battaglia
and
John Newman

Department of Chemical Engineering
University of California

and

Materials Sciences Division
Lawrence Berkeley Laboratory
University of California
Berkeley, California 94720

July 20, 1993

This work was supported by the Assistant Secretary for Conservation and Renewable Energy, Office of Transportation Technologies, Electric and Hybrid Propulsion Division of the U. S. Department of Energy under Contract No. DE-AC03-76SF00098.

Modeling of a Growing Oxide Film: The Iron/Iron Oxide System

Vincent Battaglia and John Newman

Department of Chemical Engineering, University of California, and the Material Sciences Division, Lawrence Berkeley Laboratory, University of California, Berkeley, California 94720

Abstract

The full set of equations necessary for describing the growth of an oxide film is presented. The analysis includes methods of combining equations for systems with rapid kinetics and a derivation of the high-field equation. The boundary conditions on the flux equations, Poisson's equation, and the velocity of the interface are also discussed. The methodology is then applied to the iron/iron oxide system, including reactions of electrons and iron interstitials at the metal/oxide and oxide/solution interfaces. Simulations, using the low-field equation, are compared to experimental results. It is found, in agreement with experiments, that passivation does not occur until 200 mV above the potential where the formation of an oxide is thermodynamically possible. This results because the oxide formation reaction is overwhelmed by the fast kinetics of the iron dissolution to ferrous ions.

Introduction

Oxide films are present on nearly all metal surfaces subjected to oxidative environments. Those films that are compact and poor current

conductors are referred to as passivating films. Experimentally it has been shown that passive films on metals, subject to an anodic current or potential, grow with a thickness that is roughly proportional to the logarithm of time. For over fifty years, many theories have been proposed that predict such a growth rate; and still, the most prominent theories today are but subtle improvements of some of the earliest work. (Reviews of the experiments and theories can be found in Young,[1,2] Vetter,[3] and Choa *et al.*[4])

In 1935 Verwey[5] proposed that the anodic growth of oxides is limited by the rate of transport of cationic interstitials. The driving force for migration is described by a high-field mechanism, which is exponentially dependent on the local electric field. Cabrera and Mott[6] agreed that ionic transport is dominated by cation migration by a high-field mechanism, but argued that the rate of film growth is limited by the reaction rate at the metal/oxide interface. Fehlner and Mott[7] stated that ionic transport is dominated by the conduction of anions and that the limitation to growth is the reaction rate at the oxide/solution interface. Maurer[8] suggested that the electric-field-dependent production of Frenkel defects — interstitials formed within the oxide by a field assisted jump of an ion from a lattice site — is the rate limiting step to forming mobile cationic species.

These theories have since been used as they stand, or combined to describe multiple phenomena, or slightly modified to fit particular system data. Vermilyea[9] modified the high-field theory to describe the transport in Ta_2O_5 films to include two consecutive energy barriers to ionic transport. Burnstein and Davenport[10] adjusted the high-field

model by developing an improved integration of the high-field equation. Cahan *et al.*[11] argued that the passive film on iron consists of Fe^{2+}, Fe^{3+}, and Fe^{4+} cations, the concentrations of which vary across the film due to the presence of a strong electric field. This description is then used to characterize properties of the film and its growth. Bean *et al.*[12] relied on a combination of cation interstitials formed through Frenkel defects and a high-field mechanism to describe the growth kinetics of tantalum oxide whereas Odynets[13] claimed that the creation of defects at the interface and subsequent transport across the film are equally responsible for the limited rate of film growth. Many researchers, such as Dewald,[14,15] Dignam,[16] and Greyling *et al.*,[17] ascribed the differences between experimental data and the high-field transport model to neglect of the space charge in the oxide, while others[18,19] have suggested that the data can be explained by a place-exchange model.

More recent work relies on the use of a defect model, originally developed by Frenkel.[20] This model emphasizes that current is conducted by mobile charged defects. Macdonald's point-defect models[4,21,22] do not include a high-field mechanism of migration, and only the most recent paper attempts to include finite interfacial kinetics. MacDougall's point-defect models[23,24] are concerned mostly with the structure of the oxide and suggest that transient changes of currents at a given potential are due to a reduction of the number of oxide imperfections. The models of Macdonald and MacDougall were recently compared by Dagan and Tomkiewicz[25] for the growth of films on permalloy. They found that Macdonald's model did not fit the data as well as

MacDougall's (although, MacDougall's paper is based solely on qualitative arguments).

In each of the above theories, only one mechanism at a time is considered such that an analytic expression for film growth is derived. These equations usually take one of the following forms: a logarithmic growth law, an inverse logarithmic growth law, or a modified inverse logarithmic growth law. Lukac *et al.*[26] have gone on to show that these three laws can equally describe the growth kinetics and that none of the models is completely consistent with the experimentally observed temperature and potential dependences.

We believe that any or all of the above mentioned phenomena may play a significant role in oxide growth, where the predominant mechanism is a function of the system being examined and the stage to which growth has transpired. Therefore, in order to follow the progress of the growth of any oxide film through all of its stages, a model is developed that contains all of the physics. The equations of this model are then solved simultaneously with a computer. Starting with the framework of Macdonald's point defect model, we shall present a general model that includes any number of species that may react homogeneously and heterogeneously. The model will also include effects due to variations in the adjacent solution phase and track film growth or dissolution.

In the model development we shall consider only those species that are typically present. We shall then provide the equations necessary to describe the system and touch on thermodynamic consistency. Upon completion of the general model development, we present results specific to the iron/iron oxide system. The first thing to be considered, however,

is a description of the system.

General System Description

Figure 1 provides a schematic of the system. (This figure is similar to that introduced by Vetter,[3] figure 328.) A metal substrate interacts with a solution through an oxide. The interaction is described by reactions at both interfaces, the properties of the oxide, and the properties of the solution. A one-dimensional model is developed. Furthermore, we assume that an oxide is present from the start, ignoring initial oxide formation (which, rigorously, occurs through nucleation sites and is inherently two-dimensional. A mathematically one-dimensional description of a film formed on a bare metal surface has been developed by Russell and Newman.[27])

Transport in an oxide can be interpreted in terms of mobile vacancies and defects; see Wagner.[28] A general model of an oxide must have the flexibility to accept various types of defects and associated reactions. Moreover, oxides may also be semiconductors; thus, electrons and holes as well as any dopant species must also be easily incorporated into the model. An account of the dominant modes of conduction in oxides can be found in Shewmon[29] and Sørensen.[30]

To simplify the description while still providing a general framework, we shall consider only the following charge carriers: anion and cation vacancies, anion and cation interstitials, and electrons and holes. Again, we assume that the lattice itself has no charge: only the defects possess charge. More specifically, the oxide shall be viewed as an MO background (a schematic of which appears in figure 2), where

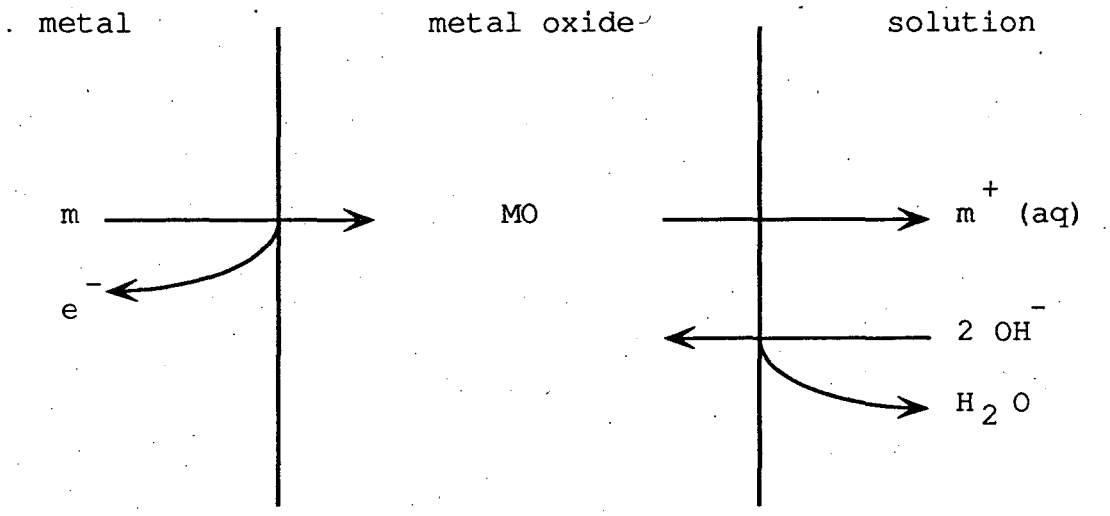

Figure 1. System.

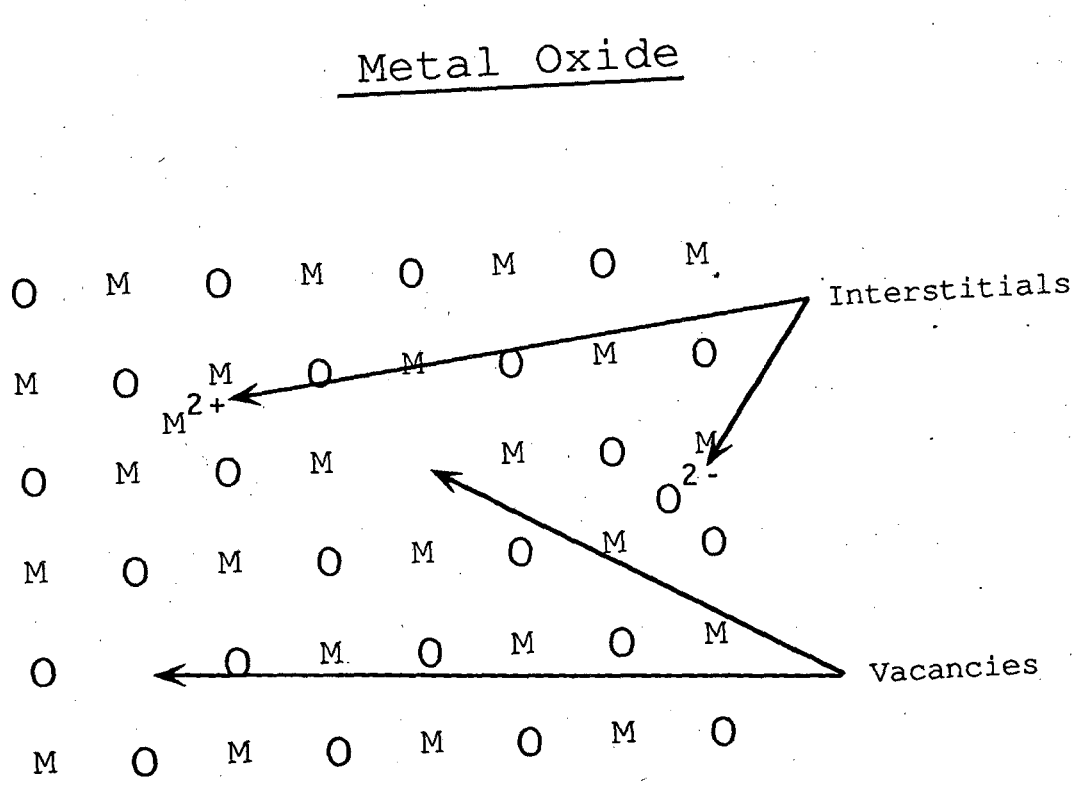

Figure 2. Schematic of an MO oxide.

cations and anions assume their respective lattice sites, are absent from their sites, or take up interstitial locations. Kroger-Vink notation is adopted for distinguishing the species. As Choa *et al.*[4] explain, X_Y denotes an X site occupied by a Y species. Hence, $V_M^{\chi-}$ describes a metal vacancy carrying χ negative charges. Following this criterion, a cation of charge 2+ in a cation site, a cation vacancy, and a cation interstitial are denoted as M_M, V_M^{2-}, and I_M^{2+}, respectively. Analogous notation is used for the anionic species. Electrons and holes appear as e^- and h^+, respectively. For our simplified description, this leads to the following types of species:

$$e^- \quad h^+ \quad V_M^{2-} \quad V_O^{2+} \quad I_M^{2+} \quad I_O^{2-} \quad M_M \quad O_O$$

We shall now consider the equations necessary to describe a system consistent with this construct.

Equations

Mole flux balance.—A mole flux balance for each species above may be written as

$$\frac{\partial c_k}{\partial t} + \nabla \cdot N_k = -\sum_{\ell} s_{k,\ell} R_{\ell}. \tag{1}$$

The reaction rate can normally be written as the difference of forward and backward reaction terms which are a function of the activities of the species (see Newman,[31] chapter 8).

For a dilute species (which excludes M_M and O_O), the flux can be written as the sum of fluxes created by separate driving forces, plus a convective term.

$$N_k \equiv c_k v_k = \text{diffusion} + \text{migration} + \text{convection} \qquad (2)$$

The convective term is defined as the concentration of the species times a reference velocity, chosen for convenience.

The diffusion and migration terms can be interpreted as a reaction. For example, the mechanism of the transport of a cation interstitial may be depicted as an interstitial at position α combining with open interstitial site at position δ to form an interstitial at position δ and an interstitial site at position α,

$$(I_M^{2+})^{\alpha} + I_S^{\delta} \rightleftarrows I_S^{\alpha} + (I_M^{2+})^{\delta} \ .$$

Such a mechanism can be described by an Arrhenius type rate expression (Newman,[31] chapter 23). Assuming the activity of the interstitial sites is constant, the rate of transport appears as

$$R_{trans} = kc^{\alpha}_{I_M^{2+}} \exp\left[\frac{z_k F(\Phi^{\alpha} - \Phi^{\delta})}{2RT}\right] - kc^{\delta}_{I_M^{2+}} \exp\left[\frac{-z_k F(\Phi^{\alpha} - \Phi^{\delta})}{2RT}\right]. \qquad (3)$$

The difference in the electrochemical potential at α and δ is defined as

$$\mu_k^{\alpha} - \mu_k^{\delta} = z_k F \eta_s = z_k F(\Phi^{\alpha} - \Phi^{\delta} - V^{O}), \qquad (4)$$

where V^{O} is the potential difference when the net rate of transport equals zero. In this case, V^{O} equals

$$V^{O} = \frac{RT}{z_k F} \ln\left[\frac{c_k^{\delta}}{c_k^{\alpha}}\right]. \qquad (5)$$

Substitution of these definitions into the rate expression gives the high-field rate expression

$$R_{trans} = 2k(c^{\alpha}_{I_M^{2+}} c^{\delta}_{I_M^{2+}})^{1/2} \sinh\left[\frac{\mu^{\alpha}_{I_M^{2+}} - \mu^{\delta}_{I_M^{2+}}}{2RT}\right]. \tag{6}$$

The difference in the electrochemical potential can be approximated as

$$\frac{\mu_k^{\alpha} - \mu_k^{\delta}}{a} = -\nabla\mu_k, \tag{7}$$

where a is some short distance. Substitution of this equation into the rate expression and assuming a small gradient in the electrochemical potential simplifies the rate expression to the linear form used in solution electrochemistry

$$R_{trans} = -\frac{ka}{RT}(c_k^{\alpha} c_k^{\delta})^{1/2} \nabla\mu_k, \tag{8}$$

where ka is recognized as the diffusion coefficient, D_k, in dilute solutions (Newman[31], chapter 11). Upon defining an electrochemical activity A_k according to

$$\exp\left[\frac{\mu_k - \mu_k^{\theta}}{RT}\right] = c_k \exp\left[\frac{z_k F\Phi}{RT}\right] \equiv A_k \tag{9}$$

and substituting into the rate expression, we obtain the simplified expression

$$R_{trans} = \frac{2D_k A_k}{a \exp\left[\frac{z_k F\Phi}{RT}\right]} \sinh\left[-\frac{a\nabla \ln A_k}{2}\right]. \tag{10}$$

Finally, combination of the flux terms provides the high-field flux expression

$$N_k = \frac{2D_k A_k}{a \exp\left[\frac{z_k F\Phi}{RT}\right]} \sinh\left[-\frac{a\nabla \ln A_k}{2}\right] + c_k v_{ref}. \tag{11}$$

The mole flux balance equation 1 for the dilute species can now be expressed in terms of the dependent variables: concentration, potential, and reference velocity. Before addressing the potential, we shall first describe the method of handling homogeneous reactions that occur at such rapidity as to be considered at equilibrium.

Combining equations.—In many instances, homogeneous reactions occur at such a fast rate that it is a good approximation to assume that the reaction is at equilibrium. When this is the case, the mole flux equations are combined to eliminate the presumed equilibrium reaction from all but one of the mole balance equations. Then this one equation is replaced with the equilibrium expression,

$$K_{\ell} = \prod c_k^{-s_{k,\ell}}, \tag{12}$$

where $s_{k,\ell}$ are the stoichiometric coefficients of reaction ℓ. We have designed a subroutine called "eqnprod" that sums the mole flux equations in such a way that each reaction, starting with the fastest reaction, is eliminated from every mole balance but one (if the specified reactions are not independent, multiple reactions may appear in the final form of the combined equations). This translates the set of i mole balance equations to $i-j$ equations of the form

$$-\sum_{\ell} \nu_{i,\ell} R_{\ell} = \sum_{k} \mu_{i,k} \left(\frac{\partial c_k}{\partial t} + \nabla \cdot \mathrm{N_k} \right), \tag{13}$$

and j equilibrium equations. (ν and μ are combinations of the stoichiometric coefficients derived through the elimination of the equilibrium reactions.) For those mole balance equations containing reactions that are fast but not considered at equilibrium, the equation can be divided through by the backward rate of the fast reaction. The

logarithm of this equation appears as

$$\ln K_{\ell_{max}} + \sum_k s_{k,\ell_{max}} \ln c_k = \ln\left[1 - \frac{\sum_k \mu_{i,k}\left(\frac{\partial c_k}{\partial t} + \nabla \cdot N_k\right) - \sum_{\ell \neq \ell_{max}} \nu_{i,\ell} R_\ell}{q_{k,\ell_{max}} \; k_{b,\ell_{max}} \prod c_k}\right] \quad (14)$$

The departure from equilibrium now appears as the logarithm of 1 minus a small number.

Poisson's equation.—Many oxide films, especially those that exist as compact crystal structures, possess a small number of defects, suggesting a small number of charge carriers and a large space-charge region. For a thin film, the space-charge layer may extend across a significant portion of the oxide. As Dewald[14] and others have shown, space charge in the oxide can have an appreciable effect on the growth rate of films. We shall therefore incorporate Poisson's equation into the model development

$$\nabla^2 \Phi = -\frac{F}{\epsilon} \sum_k z_k c_k. \quad (15)$$

Because a double layer also exists in the solution phase near the oxide/solution interface, Poisson's equation is also invoked in this phase, replacing the electroneutrality equation,

$$\sum_k z_k c_k = 0, \quad (16)$$

(which is often substituted, as a first approximation, for Poisson's equation in an electrolytic solution).

Velocity.—We have yet to develop an expression for the mole flux of M_M or O_O in terms of concentration and potential, nor have we defined

the reference velocity. We shall show how these two subjects are interrelated.

The diffusion of anion and cation vacancies occurs through the mechanisms

$$O_O + V_O^{2+} \longrightarrow V_O^{2+} + O_O,$$

and

$$M_M + V_M^{\chi-} \longrightarrow V_M^{\chi-} + M_M,$$

respectively. The mechanism for anion transport can be described mathematically as,

$$N_{O_O} - c_O v_L = -(N_{V_O^{2+}} - c_{V_O^{2+}} v_L). \tag{17}$$

The flux of V_O^{2+} relative to the convective flux is equal and opposite to the flux of O_O relative to its convective flux. An analogous relationship applies to the transport of the cation. Rearrangement of these equations leads to the definition of the lattice velocity

$$v_L \equiv \frac{\sum_{i}^{\text{O sites}} N_k}{c_O^o} = \frac{\sum_{i}^{\text{M sites}} N_k}{c_M^o} = \frac{\sum_{i}^{\text{all sites}} N_k}{c_{MO}^o}, \tag{18}$$

where c_O^o, c_M^o, and c_{MO}^o are the concentrations of O, M, and MO sites, respectively, and are constants. Summation of the mole flux balance equations over the species occupying O, M, or both sites leads to the single equation

$$\nabla \cdot v_L = 0. \tag{19}$$

This is a continuity equation consistent with the notion that the site density is constant.

In the solution, the equations that describe the velocity are the momentum-balance equations. We would prefer not to solve these equations, and instead enter velocity profiles that have been determined analytically. We shall assume that the oxide is growing on a rotating disk electrode and use the high Sc number approximation to the normal component of the velocity relative to a disk with no lateral velocity (Newman,[31] chapter 15),

$$v_x = -0.51023\zeta^2\sqrt{\Omega\nu}, \tag{20}$$

where ζ equals $x\sqrt{\Omega/\nu}$ and x is the distance normal to the surface.

Summarizing, we have a mole balance for each minor species, Poisson's equation, and a continuity equation for the velocity. This completes the mathematical description of the transport in the bulk of the film. Completion of the problem, however, consists of a description of the boundary conditions.

Boundary Conditions

We shall now discuss the boundary conditions for a multi-phase, one-dimensional problem. One method for setting boundary conditions is to mimic the experimentalist. This procedure usually leads to the correct number of constraints. For example, when a metal surface is placed in a solution with intent to form an oxide, the composition of the solution and either the potential difference across the cell or the total cell current are at the experimentalist's control. The same conditions are applied here.

The number of degrees of freedom suggests that the boundary conditions for the oxide phase, the phase sandwiched between the metal and

solution phases, are flux relationships that relate the concentration of the species in the oxide to the concentration of the species just outside the oxide as is done in the mole flux balance equation,

$$\frac{\partial \Gamma_k}{\partial t} \pm \left(N_k - c_k v_I \right) = \sum_l s_{k,l} R_{A,l}. \tag{21}$$

(The plus sign applies to the right side of an interface.) For those species that do not react at either interface nor homogeneously, there exists an additional degree of freedom. In this instance, only the initial condition is necessary for a transient problem, but for a steady-state problem one should set either the concentration of that species at one of the interfaces or an average concentration of that species.

Poisson's equation is solved from one end of the system to the other. This second-order equation requires a specification of the potential at some position, the absolute value of which is arbitrary. For convenience, the potential at the end of the solution phase farthest from the oxide is set to zero.

Gauss's law is required at the interfaces. On the solution side of the oxide/solution interface, Gauss's law takes the form

$$\nabla \Phi^s - \frac{\Phi^s - \Phi^o}{\delta_{o/s}} = -\frac{F}{\epsilon_s} \sum_k z_k \Gamma_k. \tag{22}$$

Velocity is a relative quantity, which allows us to set its value arbitrarily at any position. In other words, we can set the velocity of any one interface or set v_L (since $\nabla \cdot \mathbf{v}_L = 0$) to a convenient constant. We set the velocity of the metal/oxide interface to zero.

The equation for the velocity of the lattice was derived by summing the mole flux equations of the species occupying lattice sites. The

boundary condition is analogously developed. Depending on whether the mole flux balance equations are on the right side or left side of the interface, summation gives

$$v_L - v_I = \pm \frac{\sum_{k}^{\text{all sites}} \sum_{\ell} s_{k,\ell} R_\ell}{c^o_{MO}} \tag{23}$$

(the plus sign applies to the right side of the interface). The right side of equation 23 can also be written as

$$\frac{\sum_{l} R_l \sum_{k}^{\text{all sites}} s_{k,l}}{c^o_{MO}}. \tag{24}$$

This indicates that film growth is realized only at interfaces where the sum of the stoichiometric coefficients of species occupying lattice sites is not equal to zero.

At the metal/oxide interface, where the velocity of the interface is set to zero, equation 23 yields the lattice velocity, v_L. At the oxide/solution interface, it yields the velocity of the interface, since v_L is known by integration of equation 19 across the oxide.

Initial Conditions

In a transient case, an initial concentration of each species is required. One way to proceed is to set the potential of the metal to the value where the film, metal, and solution exist in mutual equilibrium. (If no such potential exists, an alternative would be to solve for a quasi-steady state at a given potential.) The steady-state concentration and potential distributions are solved for at this potential. The potential is stepped to a new value, and growth of the film is

followed from this initial condition. To march through time, one can either use a Crank-Nicholson time stepping algorithm or assume quasi-steady state. The first method is a better approximation, especially for rapid film growth.

This concludes the general formalism for describing oxide film growth. We shall now apply this methodology to the specific system of iron/iron oxide in a basic solution.

The Iron/Iron Oxide System

The iron/iron oxide system has received a considerable amount of attention, dating back over 100 years. Vetter, Bonhoeffer, Weil, Franck, and Sato are just a few of the researchers who have performed numerous studies to try to elucidate the mechanism of its passivation. However, the system remains poorly understood. More recent research is centered on determining the structure of the oxide with spectroscopic techniques.[32,33,34,35]

Vetter[3] provides an excellent review of much of the early work. In this section we shall outline the information provided in his investigation and then provide a physical model that is consistent with those findings and with the defect model proposed by Wagner.[36] Finally, we shall compare results from our computer simulations with the experimental data provided by Jovancicevic *et al.*[37] and Lukac *et al.*[26]

Summary of earlier work as provided by Vetter.—The Flade potential (an experimentally measured, typically nonequilibrium, potential that marks the onset of passivation) of iron is approximately 200 mV more positive than the potential at which the oxide Fe_3O_4 is stable in a

basic solution at pH = 8.4.[38] Vetter argues that the passive film is made up of a conductive layer of Fe_3O_4 that faces the metal and a non-conducting layer of Fe_2O_3 that faces the electrolyte. As the potential of the metal in contact with the solution (no oxide present) is increased, the metal preferentially dissolves as a ferrous species. The electronically conducting Fe_3O_4 oxide, the first thermodynamically stable oxide (-600 mV *versus* the NHE), does not appear due to its rapid rate of dissolution. As the potential is further increased, the Fe_3O_4 is oxidized to Fe_2O_3. This oxide is a poor conductor and features slow dissolution kinetics. Its presence leads to passivation. The Flade potential thus falls between the potentials defined by the overall reactions[38]

$$3\,Fe + 8\,OH^- \rightleftarrows Fe_3O_4 + 4\,H_2O + 8\,e^-,$$

and

$$2\,Fe_3O_4 + 2\,OH^- \rightleftarrows 3\,Fe_2O_3 + H_2O + 2\,e^-.$$

The second reaction is approximately 200 mV more positive than the first.

Another thought provided on the 200 mV discrepancy is that Fe_3O_4 and Fe_2O_3 form mixed phases with each other. ("γ-Fe_2O_3 lacks each ninth Fe ion compared to Fe_3O_4. The O^{2-} ions have the same crystal lattice."[3]) If Fe_3O_4 is preferentially formed near the metal and Fe_2O_3 near the electrolyte, a concentration gradient of iron ions and electrons is implied. A concentration gradient of iron ions is attended by a potential gradient. It is this potential variation that constitutes the difference between the predicted thermodynamic formation of oxide

and the experimentally measured onset of passivation.

Vetter further notes that thin steady-state films (< 100 nm) form on metals when dissolution occurs simultaneously with film formation. His investigation revealed that the films on iron are between 2 and 10 nm and that 100 ±2 % of the dissolution results as $Fe^{3+}(aq)$.

Model.—Starting with the assumption that the oxide is either Fe_3O_4 or Fe_2O_3, which maintain the same lattice structure but differ by the presence of cation interstitials and electrons, and that cations are the primary mode of ionic transfer in the oxide[39] leads to the description of the oxide presented in figure 3. We are assuming that the oxide takes on the structural form of Fe_2O_3 and contains mobile Fe^{3+} interstitials and electrons.

The following reactions are used to describe the interactions of the oxide with the adjoining metal and electrolyte phases. This is in agreement with the above model description and the information provided by Vetter.

At the metal/oxide interface:

$$1.) \qquad Fe(m) \rightleftarrows I_{Fe}^{3+} + 3\,e^{-}(m).$$

$$2.) \qquad e^{-}(ox) \rightleftarrows e^{-}(m);$$

At the oxide/solution interface:

$$3.) \qquad 2\,I_{Fe}^{3+} + 6\,OH^{-}(aq) \rightleftarrows 2\,Fe_{Fe} + 3\,O_O + 3\,H_2O;$$

$$4.) \qquad I_{Fe}^{3+} + 2\,OH^{-} \rightleftarrows Fe(OH)_2^{+}(aq.);$$

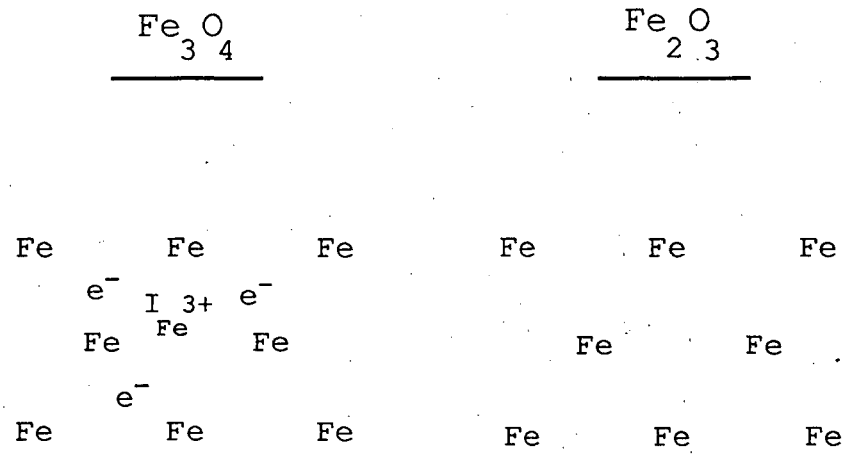

Figure 3. Schematic of iron oxide.

$$5.) \qquad I_{Fe}^{3+} + e^{-}(ox) \rightleftarrows Fe^{2+}(aq.);$$

These reactions are considered elementary reactions, and the reaction rates take the Butler-Volmer form. Equilibrium requires:

$$1.) \qquad \frac{c_{I_{Fe}^{3+}}}{K_1} = \exp\left[\frac{3F}{RT}(\Phi^m - \Phi^o)\right]$$

$$2.) \qquad \frac{1}{K_2 c_{e^-}} = \exp\left[\frac{F}{RT}(\Phi^m - \Phi^o)\right]$$

$$3.) \qquad \frac{1}{K_3 c_{I_{Fe}^{3+}}^{1/3} c_{OH^-}} = \exp\left[\frac{F}{RT}(\Phi^o - \Phi^s)\right]$$

$$4.) \qquad \frac{c_{Fe(OH)_2^+}}{K_4 c_{I_{Fe}^{3+}} c_{OH^-}^2} = \exp\left[\frac{3F}{RT}(\Phi^o - \Phi^s)\right]$$

and

$$5.) \qquad \frac{c_{Fe^{2+}}}{K_5 c_{I_{Fe}^{3+}} c_{e^-}} = \exp\left[\frac{2F}{RT}(\Phi^o - \Phi^s)\right]$$

Combinations of the elementary reactions lead to the overall reactions:

$$\frac{3}{4}Fe(m) + 2\,OH^- \longrightarrow \frac{2}{3}Fe_{Fe} + O_O + \frac{1}{12}I_{Fe}^{3+} + \frac{1}{4}e^-(ox) + H_2O + 2\,e^-(m);$$

$$Fe(m) + 2\,OH^- \longrightarrow Fe(OH)_2^+(aq) + 3\,e^-(m);$$

and

$$Fe(m) \longrightarrow Fe^{2+}(aq) + 2\,e^-(m).$$

It is these overall reactions for which thermodynamic constants can be found in the literature.

We shall now present the system parameters: how they were chosen or determined.

System parameters.—Table 1 provides a list of the mobile species and properties of the phases.[31,40] The electronic conductivity of Fe_3O_4 is high; therefore, an arbitrarily high diffusion coefficient for the electrons is chosen (100 cm^2/s, the same order of magnitude as found in some semiconductors). In the aqueous phase, we could not find the diffusion coefficient for the two boric species or the ferric species; however, since the current through passive films is low ($\approx$ 5 $\mu A/cm^2$) and limited by transport of an ion in the film, an estimate in the solution

Table 1

Phase 1: γ-Fe_2O_3

density (g/cm^3)	mol. wt. (g/mol)	dielectric coeff.
5.24	55.847	9.
Mobile Species	**Conc. (M)**	**Diff. coeff. (cm^2/s)**
I_{Fe}^{3+}	8.2	$2.\times10^{-16}$
e^-	24.6	$1.\times10^{2}$

Phase 2: H_2O

density (g/cm^3)	mol. wt. (g/mol)	dielectric coeff.
1.	18.0	78.
Mobile Species	**Conc. (M)**	**Diff. coeff. (cm^2/s)**
Na^+	0.20	1.334×10^{-5}
Fe^{2+}	3.9×10^{-6}	0.72×10^{-5}
$Fe(OH)_2^+$	1.3×10^{-18}	$1.\times10^{-5}$
$B_4O_7^{2-}$	0.0500039	$1.\times10^{-5}$
$HB_4O_7^-$	0.1	$1.\times10^{-5}$

phase should be sufficient. The diffusion coefficient of interstitials for an oxide is typically small and in this model is the mass-transfer limitation to oxide growth. The current density is limited by the rate of transport of interstitials and is directly related to the diffusion coefficient of the iron interstitials. As we shall demonstrate, this value is on the order of 10^{-16} cm^2/s.

The equilibrium constants of the elementary reactions must be consistent with the equilibrium constants of the overall reactions which are found in the literature. The three overall reactions can be in equilibrium simultaneously if we set the Fe^{2+} concentration at 3.9×10^{-6}M, the $Fe(OH)_2^+$ concentration at 1.3×10^{-18}M, the pH at 8.4, and the potential *versus* a hydrogen reference electrode in the same solution to -103 mV (-600 mV *versus* the NHE). This difference in potential is distributed across the interfaces of the system and the double layers at each interface.

We shall now demonstrate how the potential varies from the metal to the reference electrode using our best judgement and the scant data available. We expect a potential drop between the reference electrode and the solution phase. Since we are not interested in the physics in this region, we simply require an estimate of its value to subtract from the total of -103 mV. From potential-of-zero-charge data of the hydrogen/mercury reference electrode, it is estimated that the potential difference between the electrode and the solution is -248.2 mV. Adding this potential to the potential difference from the metal to the reference electrode gives a potential difference from the metal to solution of -351.2 mV.

The iron phase adjacent to the oxide can be thought to consist of iron ions and electrons. Since these two species are the only mobile species in both the oxide and metal phases, we shall assume that the equilibrium potential drop across this interface is zero.[41] We are left with distributing the -351.2 mV between the oxide and the solution. We do not have information on the absorption equilibrium constants of the electrons, interstitials, sodium ions, ferrous ions, *etc.* at the oxide/solution interface; therefore, we shall assume that there is no specific absorption of any of the species on either side of this interface. We shall also assume that the interfacial region has a finite thickness of 0.35 nm and a dielectric constant that is equal to the average of the dielectric constant of the two adjacent bulk phases. Although we do not account for specific adsorption, an equal and opposite amount of diffuse charge accumulates on each side of the interface to account for the potential variation and satisfy Poisson's equation.

The equilibrium constants of the five reactions must be consistent with the equilibrium constants of the three overall reactions. This leaves us with two degrees of freedom. The assumption that the equilibrium potential drop across the metal/oxide interface is zero eliminates one degree of freedom, and the assumption that the concentration of iron interstitials is equal to the bulk concentration of iron interstitials required to make the Fe_2O_3 lattice structure into Fe_3O_4 (which is 8.2 M) eliminates the second degree of freedom. These values are substituted into the first equilibrium relation to obtain K_1. The concentration of electrons is related to the concentration of interstitials through electroneutrality, thus, K_2 is determinable. Substituting into the last

three equilibrium relations the bulk concentrations and potentials provides the remaining three equilibrium constants. The equilibrium constants of reactions 1, 2, 3, 4, and 5 are accordingly

$$K_1 = 0.04065 \text{ 1/mol}, \quad K_2 = 8.2 \text{ mol/l}, \quad K_3 = 8.57272 \times 10^5 \text{ (1/mol)}^{1/3},$$

$$K_4 = 4.07739 \times 10^{-1} \text{ 1/mol}, \quad \text{and } K_5 = 1.44466 \times 10^4 \text{ 1/mol}.$$

We shall now present the results of our simulations and discuss the attributes and inadequacies of the model as compared to experimental findings.

Results and Discussion

The growth of an oxide on iron in a basic medium of boric acid and sodium borate, pH of 8.4 is predicted by computer simulation. Generated curves will be compared to experimental data. It is not our intention to present a parametric study of the diffusion coefficients and the rates of the interfacial reactions. For this reason we shall present only our best fits to the experimental data and simply describe the results of varying certain parameters. For easy comparison to experimental data, the simulations are corrected by 248.8 mV such that the potential of the metal is consistent with the potential one would read *versus* the NHE.

Equilibrium.—The first result is the potential distribution for the equilibrium conditions. The system consists of a 0.1 nm thick oxide sandwiched between an iron surface to the left and a borate buffer solution to the right. The metal phase is set to the equilibrium potential of −600 mV (with the correction as discussed above) *versus* the potential

of the solution of −248.8 mV at a point just outside the mass-transfer boundary layer, 12.6 μm thick. The potential distribution across the oxide and solution phases is plotted against the position from the metal surface divided by the width of the particular phase, figure 4. The potential varies by approximately 47 mV in the double layer of the oxide at the oxide solution/interface and varies by approximately 104 mV through the double layer of the solution phase near this same interface. The rest of the 351 mV is across the oxide/solution interface.

The potential distribution in the solution appears to drop straight down at the interface. This is an illusion created by the thinness of the solution double layer (0.61 nm) compared to the width of the mass-transfer layer (12.6 μm). The potential distribution in the oxide also reveals the thinness of the oxide double layer: about 0.015 nm. This is considered small for most oxide semiconductors but agrees with the notion of Wagner[36] for this oxide. The corresponding concentration profiles of the electrons and interstitials in the oxide are provided in figure 5. The concentration of the electrons increases by a factor of 10 near the interface, and the concentration of the interstitials drops by nearly two orders of magnitude. This is a function of the potential dependence of the concentrations as given above. Figure 6 provides the concentration and potential profiles in the solution phase *versus* the dimensionless coordinate y. This blown up view shows the curvature of the potential through the double layer near the interface and the corresponding concentration profiles. The concentrations in this region similarly obey the potential dependence given above.

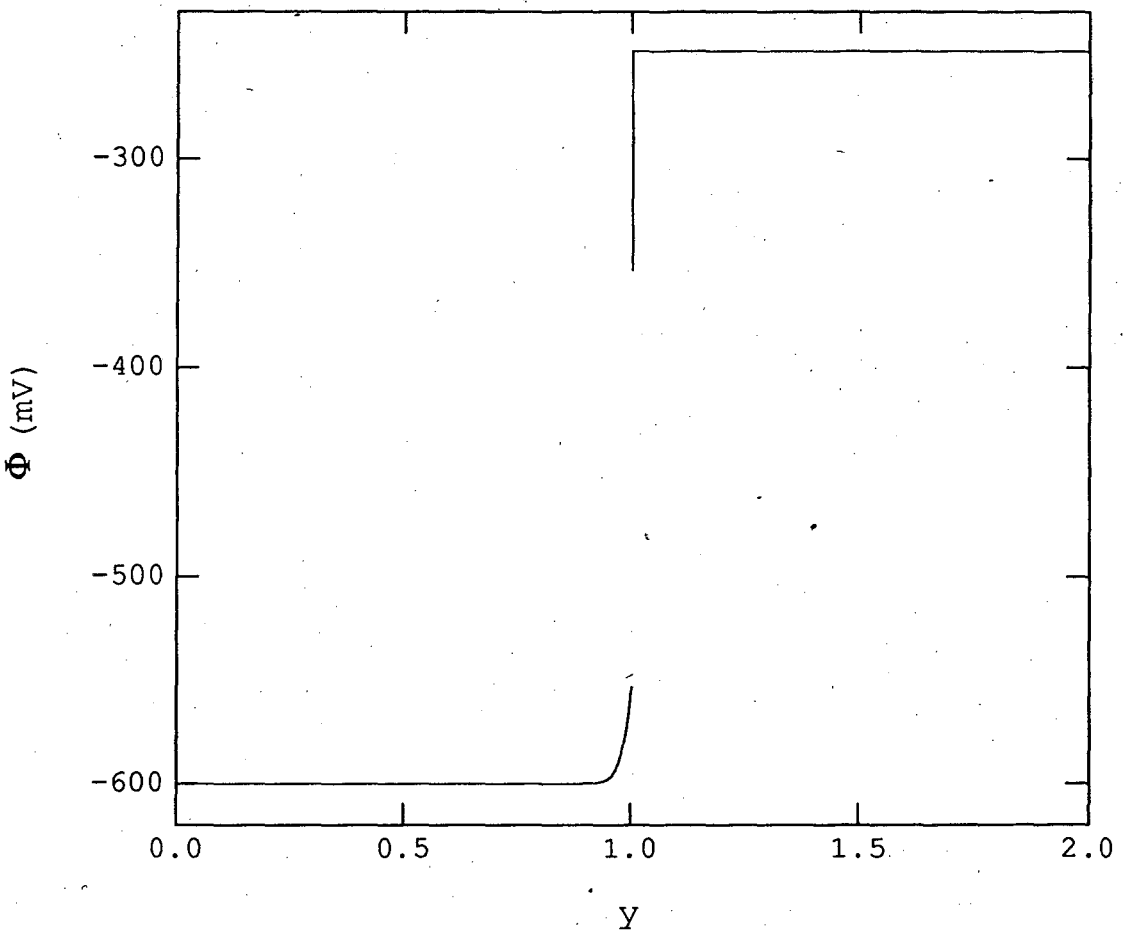

Figure 4. Potential distribution across the oxide and solution phases at the equilibrium potential, V = -600 mV *vs.* the NHE.

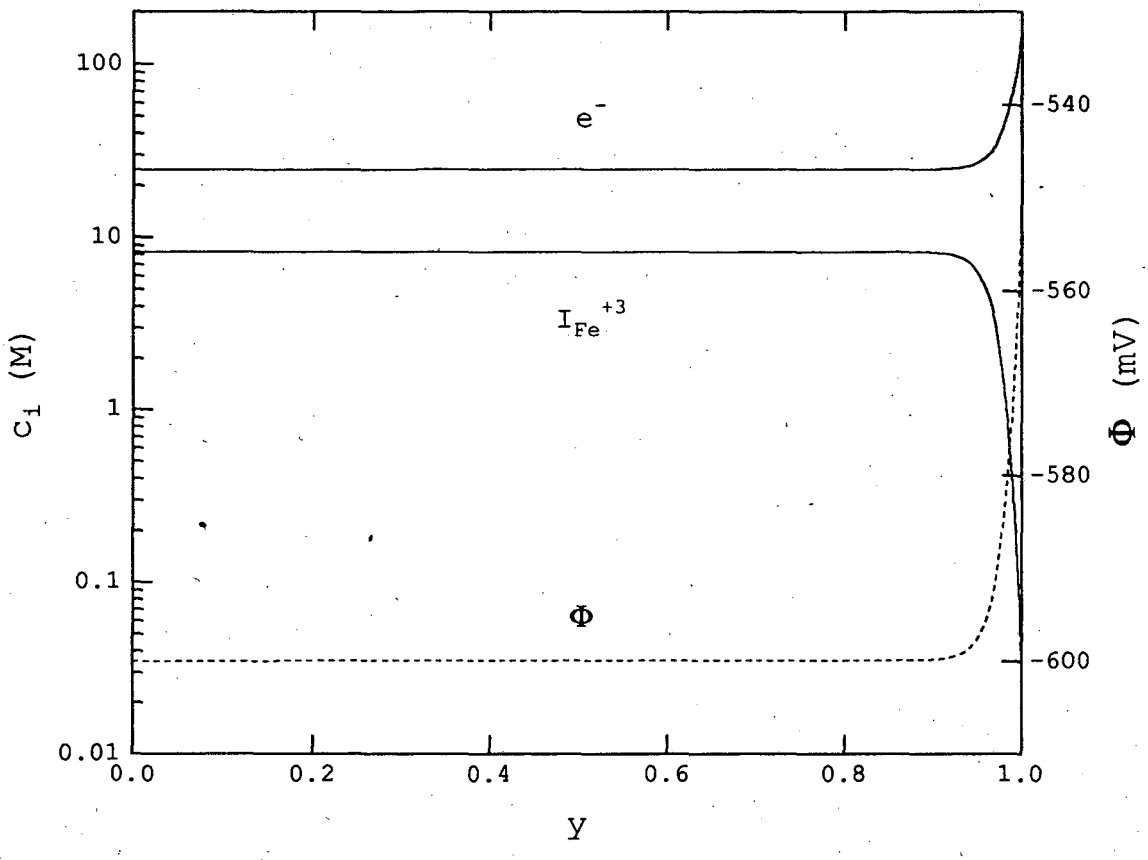

Figure 5. Potential and concentration distributions of interstitials and electrons *versus* the dimensionless coordinate, *y*, at the equilibrium potential, V = -600 mV *vs.* the NHE.

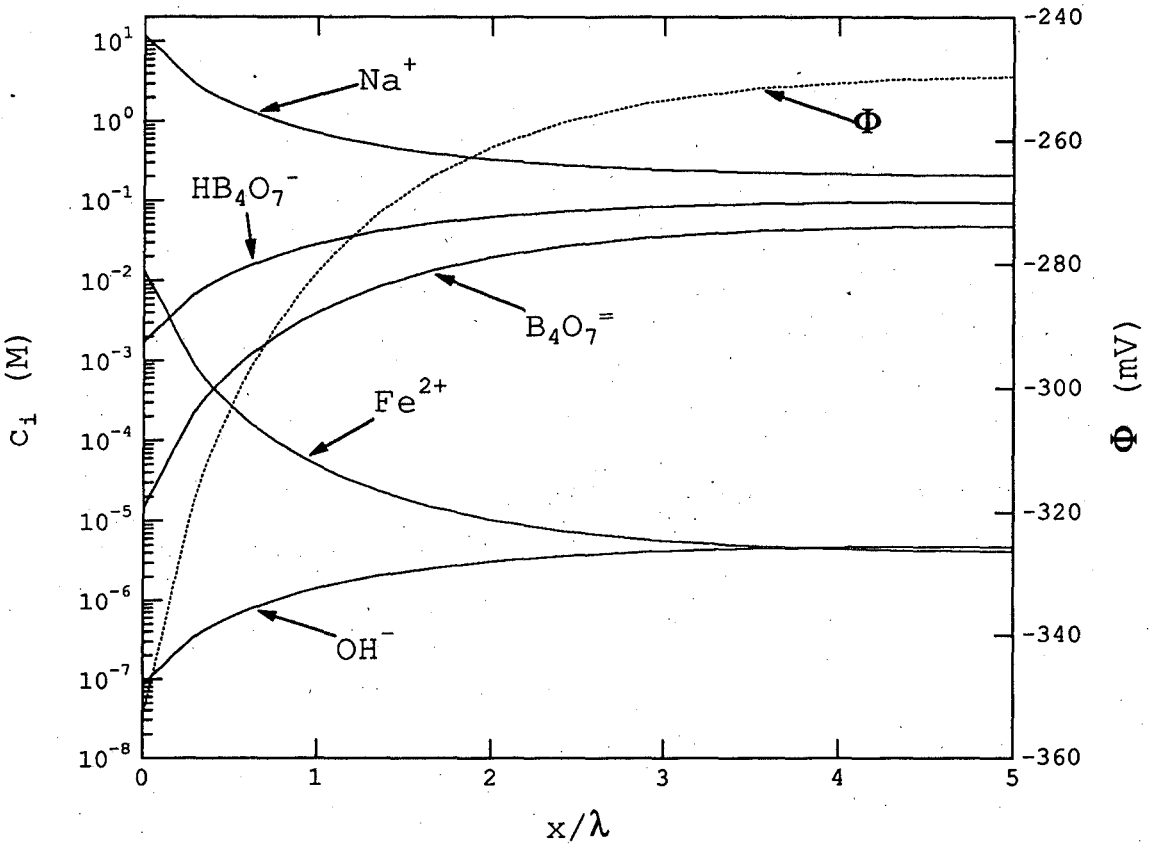

Figure 6. Concentration and potential distributions in the solution phase at the equilibrium potential *versus* the number of debye lengths from the oxide surface. V = -600 mV *vs.* NHE.

The next results describe the growth of the oxide during a positive sweep of the potential.

Comparison with experimental data.—In this part of the investigation, we introduce curves of current and length *versus* potential. The curves presented are those that best fit the experimental data in the literature with emphasis on important aspects of the effects of varying certain parameters. Also shown are results that include additional physics, performed to augment the comparison with the data.

We were unable to implement the high-field rate equation. The severe nonlinearity of this equation, combined with the high degree of coupling of Poisson's equation and the flux equations provided too difficult a challenge for Autoband[31] (the numerical differentiation subroutine we chose for solving the equations). The following results were obtained using the small gradient approximation of the high-field equation. It is felt that many of the trends seen in the low-field regime should hold in the high-field regime.

Figure 7 contains experimental data reproduced from Jovancicevic *et al.*[37] The current *versus* potential is featured for a sweep rate of 0.3 mV/s. Also shown in the figure is a computer generated simulation for the same sweep rate assuming a quasi-steady state. According to Jovancicevic *et al.*,[37] an oxide of 0.03 nm is not seen until the potential equals -500 mV (this is 100 mV above the equilibrium potential). Since we have not included nucleation in the model, we cannot simulate the results of a zero thick oxide. The simulations therefore start at -500 mV. The 0.03 nm measured at this potential is thinner than an atom, and probably means that roughly 30% of the film is covered by a 1 nm thick

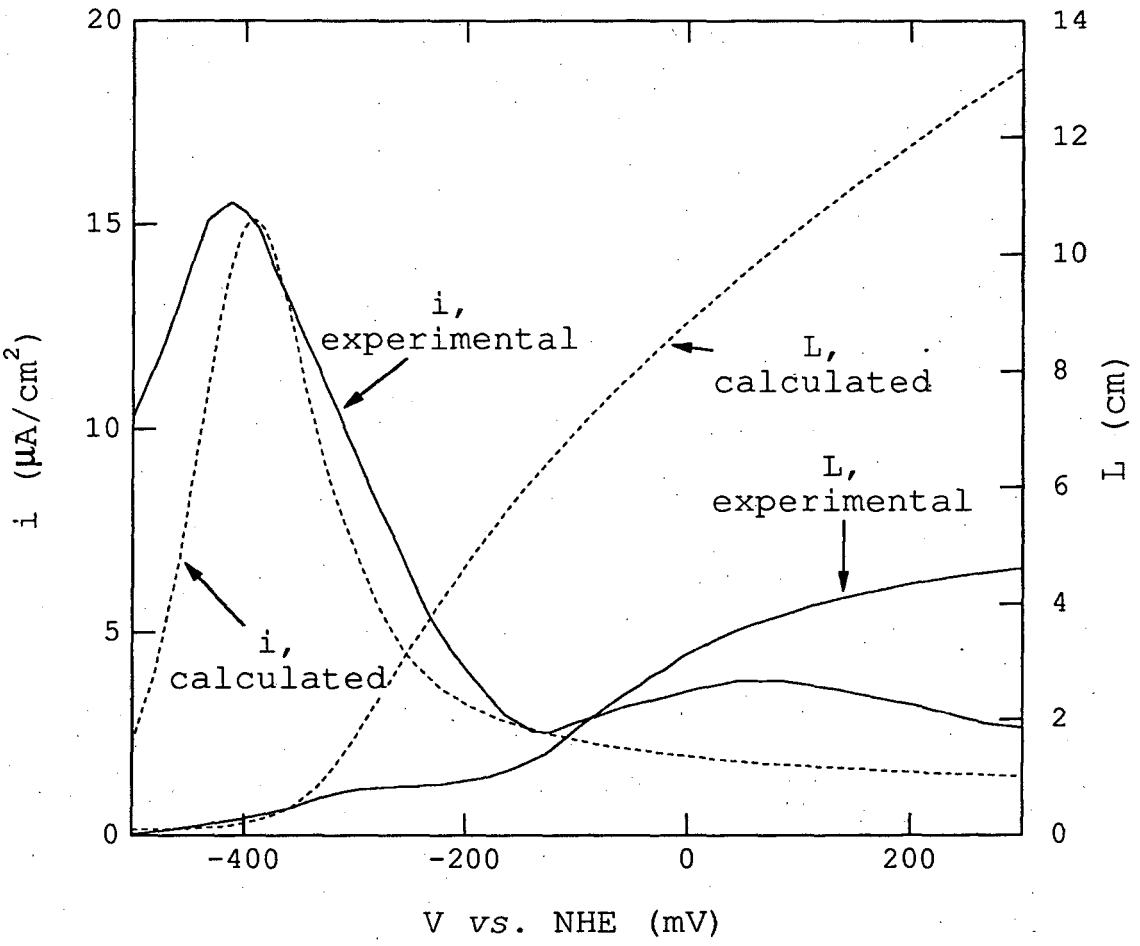

Figure 7. The solid curves are current and length *versus* potential data at 0.3 and 5.0 mV/s, respectively, from Jovancicevic *et al.*[36] The dashed curves are current and length *versus* voltage at 0.3 mV/s from simulations.

film. Our model does not include nucleation or a means of handling the kinetics of partial coverage. The simulation will therefore provide a poor fit at the lower potentials.

To fit a curve to the data, we have at our disposal five rate constants and the diffusion coefficients of the species in the oxide. The diffusion coefficient of the interstitials is much smaller than that of any other species, and the interstitials are involved in all of the proposed reactions. It is therefore the only diffusion coefficient that we shall adjust.

The electrons move relatively easily through the oxide and, we assume, pass easily into the metal phase. Reaction 2 is therefore assumed to progress at a high enough rate to be considered at equilibrium. A variation of the rate of interstitials from the metal into the oxide should equally affect the flux of interstitials to the opposite interface. Thus, to avoid needless complications, we assume that the rate of reaction 1 progresses fast enough to be considered at equilibrium. Simulations show that the equilibrium constant for the ferric reaction, reaction 4, is too low to have an effect, independent of its rate. For this reason the reaction is assumed to be at equilibrium (hence, maximum rate). This reduces our flexibility to varying two rate constants, of reactions which occur at the oxide/solution interface, and the diffusion coefficient of the interstitials.

Simulations showed that as the rate constant of the ferrous reaction, reaction 5, is increased, the initial peak in the current in figure 7 moves up and to the right with respect to potential. An increase in the oxide-forming reaction, reaction 3, has the opposite effect. The

diffusion coefficient of the interstitials moves the entire curve vertically up or down in a manner that is proportional to the change in the diffusion coefficient.

Initially, as the current increases with potential, the current is limited by the rate of the ferrous reaction. The oxide-forming reaction also increases with potential, although it is not the dominant reaction, and the oxide thickens. When the current reaches a peak, the system is switching from a reaction-limited regime to a diffusion-limited regime, which defines the onset of passivation. In this regime, the current density decreases as the oxide thickens. In the diffusion limited regime, the interstitials reach the surface at some finite rate. The interstitials are then consumed by one of the three reactions at the oxide/solution interface. As the potential is increased, the reaction that consumes the majority of interstitials shifts from a reaction of lower charge transfer to one of higher charge transfer. The charge transfer number of reaction 5 is equal to two, and the charge transfer number of reactions 3 and 4 is equal to three. Between reactions of the same order, the reaction with the combination of equilibrium constant and rate of reaction that allows it to appear first as the dominant means of interstitial consumption, continues to prevail at higher potentials. For these reasons we see in figure 8 that the dominant rate of interstitial consumption switches from reaction 5 to reaction 3. The equilibrium constant of reaction 4 is too small to allow it to compete with reaction 3, although at the higher potentials reaction 4 carries more current than reaction 5.

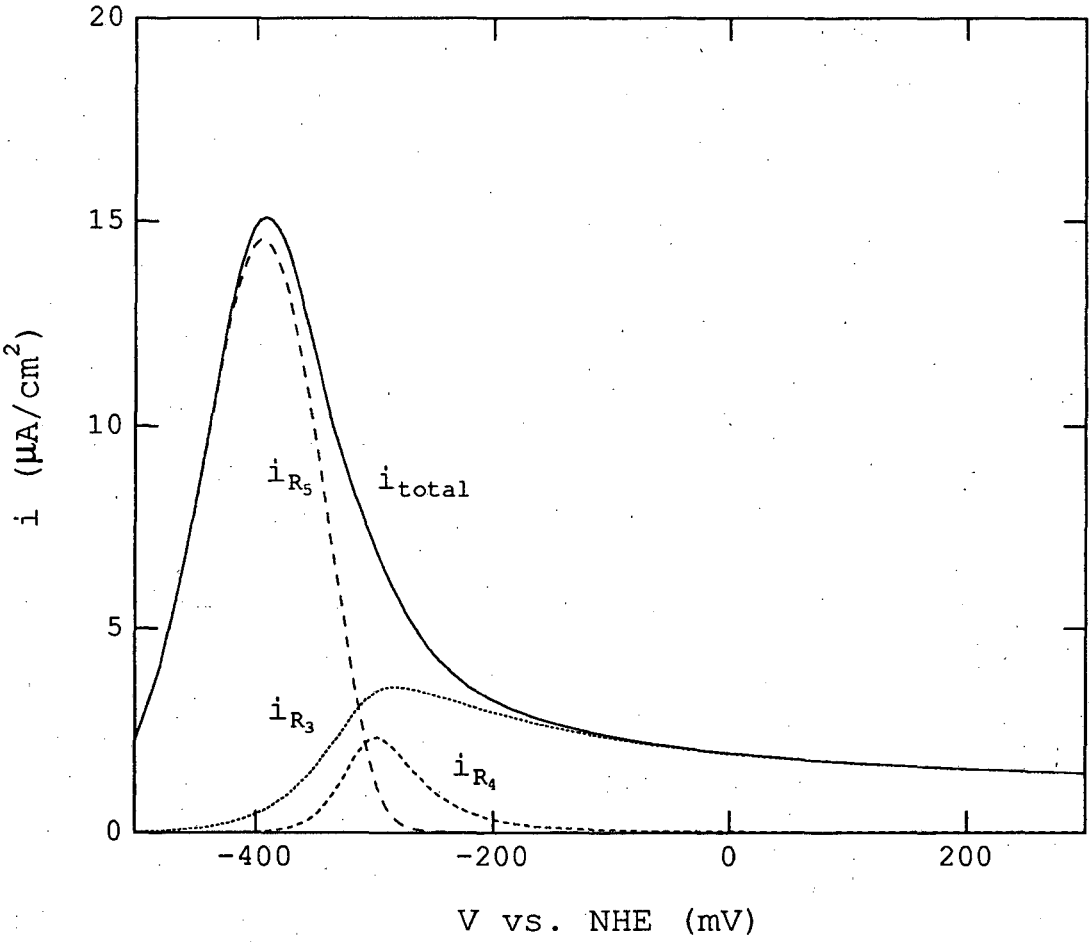

Figure 8. The currents through each reaction at the oxide/solution interface *versus* the potential. Sweep rate = 0.3 mV/s.

If the oxide were electrically neutral and the flux of electrons were equal to zero, the limiting current would obey the equation

$$i_{lim} = 3FN_{I_{Fe}^{3+}} = 3F\left(\frac{4D_{I_{Fe}^{3+}} c_{I_{Fe}^{3+}}}{L}\right), \tag{25}$$

where the concentration of interstitials is that at the metal/oxide interface. The diffusion-limited current of interstitials that are initially consumed primarily by the ferrous reaction is accompanied by a flux of electrons of the same direction and magnitude. The current carried by the electrons, however, is of the opposite sign and one third of the interstitial current. Thus, the limiting current appears as two thirds of that expected from the diffusive flux of interstitials alone. Figure 9 presents the current from the simulation and the theoretical limiting current and two-thirds of the theoretical limiting current when electroneutrality holds. This transition from a limiting current of interstitials accompanied by electron transport to the limiting current with no electron transport should follow the transition of the current from the ferrous reaction to the oxide-forming reaction. We therefore expect the two-thirds limiting current to lie on top of the simulation current at the potential where the peak starts to turn down and the full limiting current line to coincide with the simulation current at higher potentials. The lack of agreement at the low-potential end occurs because the growth rate of the oxide causes the current to be smaller than that calculated solely from the diffusion coefficient and the instantaneous film thickness.

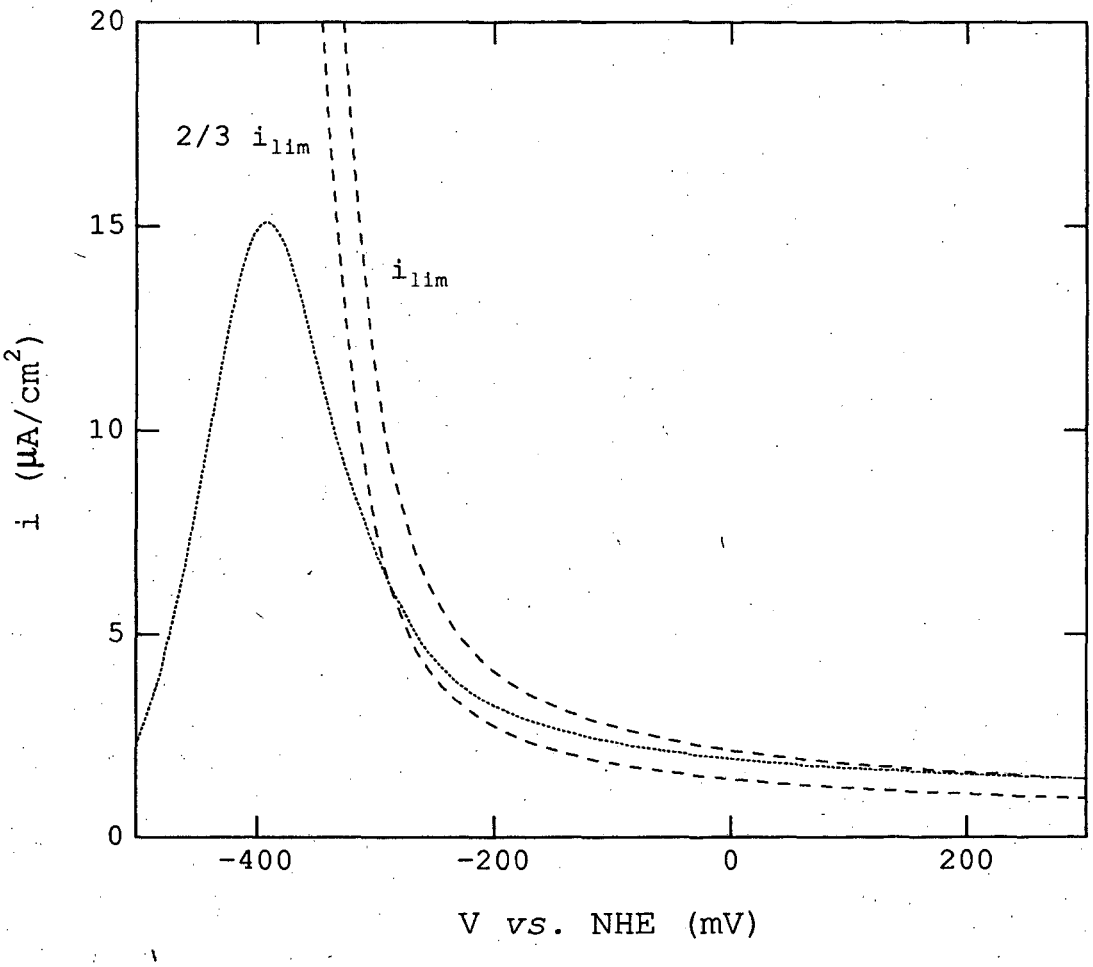

Figure 9. Current *versus* potential from simulation and an estimate of the limiting current and two-thirds of the limiting current. Sweep rate = 0.3 mV/s.

In the end, the values that provide the best fit to the data are

$$k_{-3} = 1\times10^{-13}\ \text{mol/cm}^2\text{-s},\ k_{-5} = 1\times10^{-11}\ \text{cm/s},\ \text{and}\ D_{I_{Fe}^{3+}} = 2\times10^{-16}\ \text{cm}^2/\text{s}.$$

Further inspection of the data provided by Jovancicevic *et al.* reveals a peak in the current at a potential of around 100 mV. Our first inclination was that this is the result of another reaction, perhaps the ferric reaction, reaction 4, becoming the dominant means of interstitial utilization. The simulations above were obtained assuming that reaction 4 is at equilibrium. It is therefore impossible to increase the rate of this reaction. But perhaps the equilibrium constant reported for this reaction was incorrect, and maybe there is room for adjusting its value. However, this reaction has the same reaction order as that of the oxide-film reaction. Therefore, the equilibrium constant must be increased to the point where the rate of reaction 4 overcomes the rate of reaction 3, the oxide-forming reaction. If this is done, the oxide-film reaction is diminished, and the current continues to increase with potential, switching from the ferrous reaction to the ferric reaction. Eventually, enough oxide would be formed at the slow reaction rate to limit the rate of transport of interstitials, and the current would slowly decrease. The final result would still be one large peak in the current.

Underpotential deposition.—The thickness of the oxide measured *versus* the potential during a sweep rate of 5 mV/s is provided in figure 7. A plateau in the oxide thickness at around 7.5 nm appears between -375 and -175 mV. This leads us to believe that there may be underpotential deposition. Underpotential deposition (UPD) is the deposition

of any solid on a substrate made of a different material than the deposit where the substrate is thermodynamically more stable for deposition than the deposit. Deposition of this type is analogous to the BET isotherm where the surface coverage of gas molecules is a function of the pressure of the surrounding gas. We would like to take advantage of this similarity and use the equations previously derived in the literature for the BET isotherm. A driving force for deposition that is a function of the thickness of the oxide is subsequently developed and included in the oxide-forming reaction; see the Appendix.

The result of the adjustment to reaction rate 3 to include UPD on the current and the length of the oxide when the potential is swept at a rate of 0.3 mV/s is provided in figure 10. One sees a peak in the current at the same potential where the length of the film briefly levels off. The peak in the current appears because the oxide stops growing, and thus, the diffusion-limited current stops decreasing. The current tends to level off. A few millivolts further to the right in figure 11 the oxide film reaction begins to increase again, while the current drops off again.

The reason we included UPD in this analysis was not only to make the length *versus* potential curve agree with the experimental data but also to get the second peak in the current to agree as well. The peak we get is nowhere near the potential of the second peak in the experimental data. In the simulations, the leveling off of the oxide is going to appear at the same potential where the peak in the current appears. In the experiments, these two phenomena are separated by 200 mV. We conclude that the two events in the data are mutually exclusive. With

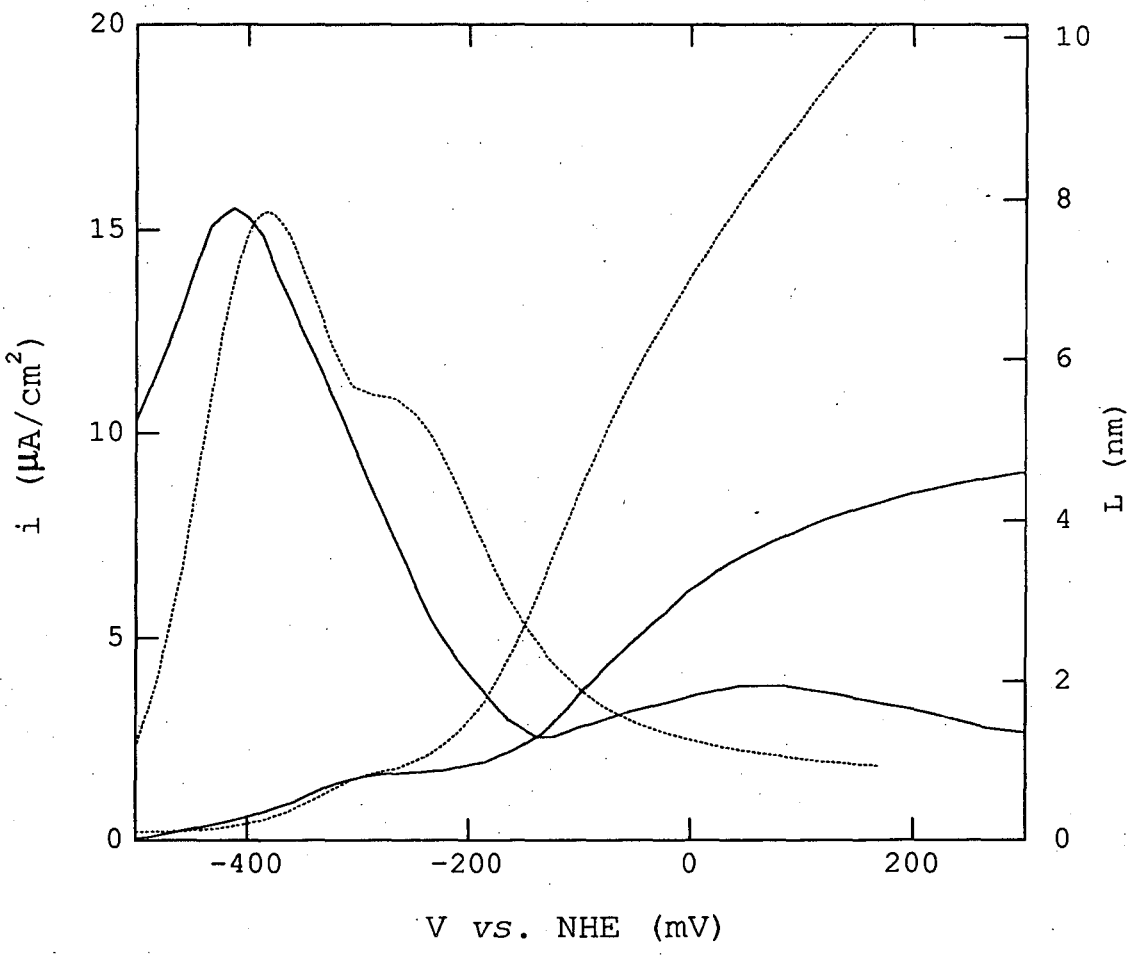

Figure 10. Solid curves are current and length *versus* potential data at 0.3 and 5 mV/s, respectively, from Jovancicevic *et al.*[36] The dashed curves are current and length *versus* voltage at 0.3 mV/s from simulations that include UPD.

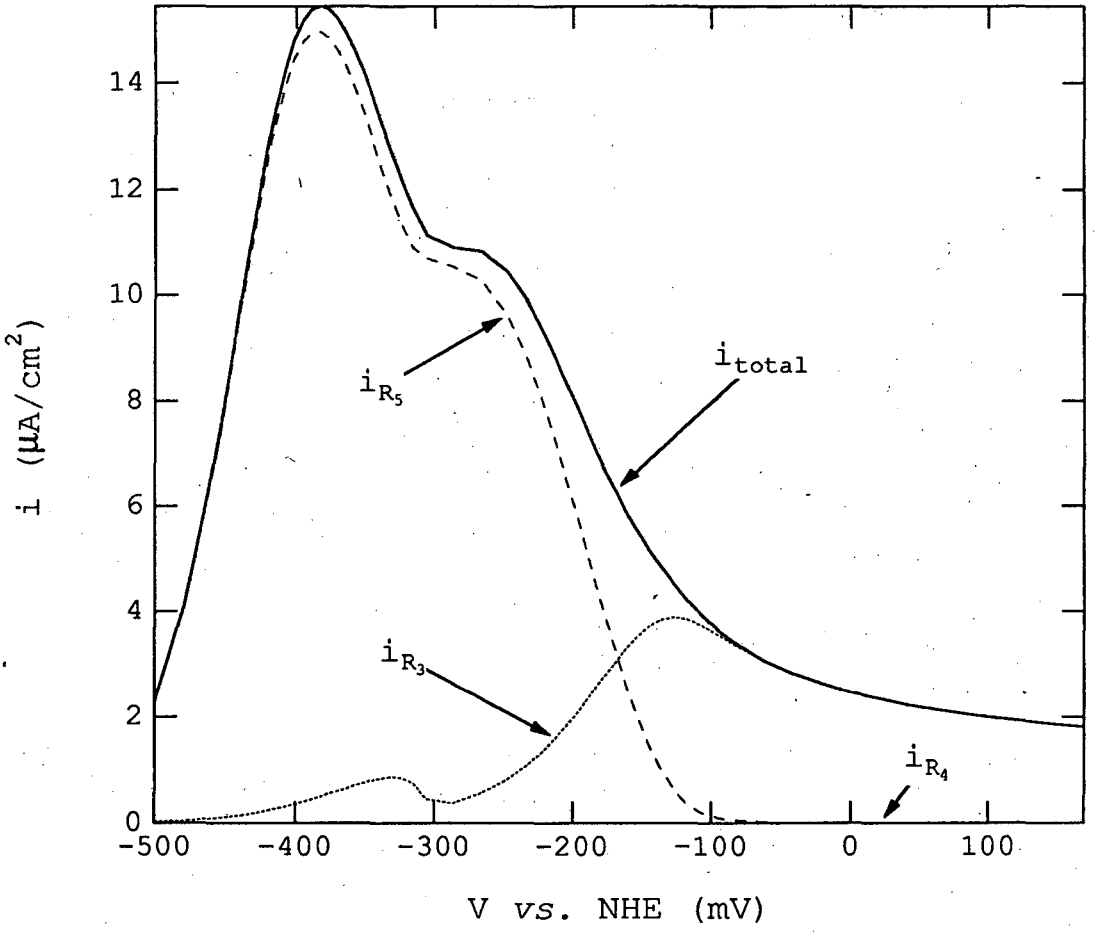

Figure 11. The currents through each reaction at the oxide/solution interface *versus* the potential with UPD. Sweep rate = 0.3 mV/s.

the present amount of physics included in this analysis, it is impossible for us to match all of the data provided by Jovancicevic *et al.*

A final comparison to experimental data is provided. Included in figure 12 are the data from Jovancicevic *et al.*, our original simulation (without UPD), and the current *versus* potential curve reproduced from Lukac *et al.*[26] Our work appears to be in far better agreement with the work of Lukac *et al.* than that performed by Jovancicevic *et al.* After exhausting all physically reasonable avenues for creating simulations that could duplicate the results of Jovancicevic *et al.*, we come to the conclusion that perhaps the work done by Lukac *et al.* was done under better, controlled conditions.

Summary

We have presented the equations that describe the growth of a film. Methods of combining the equations to eliminate rapid reactions are provided, as well as the boundary conditions and a means for solving the equations. Equations that find specific application to oxide films were developed as were variables that make the computation simpler. A model was developed specifically for the iron/iron oxide system. Using the low-field mole-flux equation, a comparison of simulation results is made to existing experimental data. From this analysis we conclude that as the potential of iron in a borate buffer solution is swept in an increasing manner, iron initially reacts to form dissolved ferrous species. Eventually, at approximately 200 mV above equilibrium, an oxide is formed that is thick enough to cause a switch to the mass-transfer-limited regime and the onset of passivation. At higher poten-

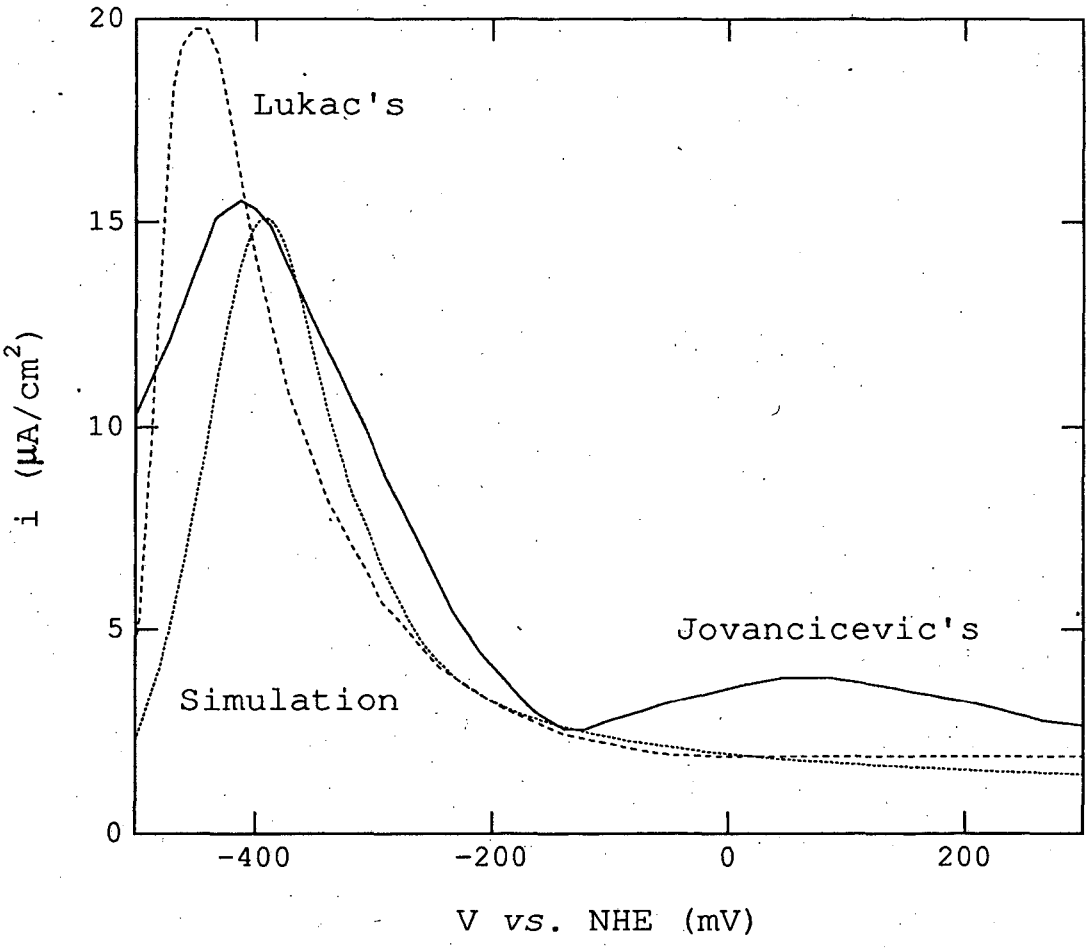

Figure 12. Current *versus* potential from Jovancicevic *et al.*[36] and the simulation at a sweep rate of 0.3 mV/s and Lukac *et al.*[25] at a sweep rate of 1/3 mV/s.

tials, the oxide-film-forming reaction becomes the dominant reaction.

List of Symbols

Roman

a	jump distance, cm
a_k	activity of species k
c_k	concentration of species k, mol/cm^3
D_k	diffusion coefficient of species k, cm^2/s
e^-	symbol for the electron
F	Faraday's constant, 96485 C/equiv
h^+	symbol for the hole
i	current density, A/cm^2
k_ℓ, $k_{-\ell}$	forward and backward rate constants of rxn. ℓ
K_ℓ	equilibrium constant of reaction ℓ
L	length of phase, cm
m	the m^{th} interface from the left
m_o	the chosen stationary interface
n	number of charges transferred in a reaction
N_k	mole flux of k, mol/cm^2-s
p_k	reaction order for forward reactants
q_k	reaction order for backward reactants
R	universal gas constant, 8.3143 J/mol-K
R_ℓ	reaction rate of ℓ, mol/cm^3-s
R_{A_ℓ}	reaction rate at surface of ℓ, mol/cm^2-s
s_k	stoichiometric coefficient of species k

t	time, s
T	temperature, K
U^{θ}	standard electrode potential, V
v	velocity, cm/s
V	electrode potential, V
x	coordinate, cm
X_Y	X site occupied by Y
y	dimensionless coordinate
z_k	charge number of species k

Greek

β	symmetry factor
δ	distance between charges in different phases, cm
Γ_k	surface concentration of species k, mol/cm^2
ϵ	permeability, F/m
ζ	dimensionless distance
μ_k	electrochemical potential of k, J/mol
ν	viscosity, g/cm-s
Φ	electric potential, V
Ω	angular velocity, s^{-1}

subscripts

i,k	species i and k
I	interface
l	reaction 1
L	lattice
migr	migration
ref	reference

superscripts

m	metal
o	oxide
s	solution
'	position to the left of x
''	position to the right of x

Acknowledgments

This work was supported by the Assistant Secretary for Conservation and Renewable Energy, Office of Transportation Technologies, Electric and Hybrid Propulsion Division of the U.S. Department of Energy under Contract No. DE-AC03-76SF00098.

Appendix

The BET isotherm[42] is

$$v = \frac{v_m c P}{(P_o - P)\left[1 + \frac{(c-1)P}{P_o}\right]}, \qquad \text{(A-1)}$$

where v is the volume of the adsorbed layer, v_m is the volume of a monolayer of the absorbed layer, c is a constant related to the heat of adsorption, and P_o is the saturation pressure. In relation to this analysis, the volume of the absorbed layer is analogous to the thickness of the oxide, L, and the pressure is analogous to the applied potential, U:

$$v \longleftrightarrow L \quad \text{and} \quad \ln\frac{P}{P_o} \longleftrightarrow \frac{nFU}{RT}.$$

We require an equation that gives the potential as a function of the length. Rearrangement of the above equation and substitution of L and U give

$$\frac{nFU}{RT} = \ln\frac{2P_o}{\left\{\left[c\left(\frac{L_m}{L} - 1\right) + 2\right]^2 + 4(c-1)\right\}^{1/2} + c\left(\frac{L_m}{L} - 1\right) + 2} \qquad \text{(A-2)}$$

c is related to the width of the potential plateau, U_o, through the equation

$$c = \exp\left(\frac{FU_o}{RT}\right). \qquad \text{(A-3)}$$

From the data of Jovancicevic *et al.*,[37] we estimate that U_o is approximately 200 mV.

The BET isotherm relates the volume of coverage to the gas pressure. The surface coverage is not strictly associated with either interface. In this analysis, a relationship between the potential of oxide deposition and the amount of coverage is also not strictly associated with either interface. However, we felt that the best way to incorporate the UPD was to attribute it to the oxide-forming reaction, reaction 3, at the oxide/solution interface. Thus, the U defined above was subtracted from the potential difference of the oxide/solution interface in both the forward and reverse reaction rates of reaction 3,

$$R_3 = k_3 c_{I_{Fe}^{3+}}^{1/3} c_{OH^-} \exp\left[\frac{(1-\beta)F}{RT}(\Phi^o - \Phi^s - U)\right] - k_{-3}\exp\left[-\frac{\beta F}{RT}(\Phi^o - \Phi^s - U)\right]. \qquad \text{(A-4)}$$

References

1. L. Young, "The Theory of Formation of High Resistance Anodic Oxide Film," *Can. J. Chem.*, 371, 276-285 (1959).

2. L. Young, *Anodic Oxide Films*, Academic Press, London (1961).

3. K. J. Vetter, *Electrochemical Kinetics. Theoretical and Experimental Aspects*, Academic Press, New York, 748-789 (1967).

4. C. Y. Choa, L. F. Lin, and D. D. Macdonald, "A Point Defect Model for Anodic Passive Films," *J. Electrochem. Soc.*, 128, 1186-1194 (1981).

5. E. J. W. Verwey, "Electrolytic Conduction of a Solid Insulator at High Fields," *Physica*, 2, 1059-1063 (1935).

6. N. Cabrera and N. F. Mott, "Theory of the Oxidation of Metals," *Repts. Progr. Phys.*, 12, 163-184 (1948-49).

7. F. P. Fehlner and N. F. Mott, "Low-Temperature Oxidation," *Oxidation of Metals*, 2, 59-99 (1970).

8. R. J. Maurer, "Deviations from Ohm's Law in Soda Lime Glass", *J. Chem. Phys.*, 9, 579-584 (1941).

9. D. A. Vermilyea, "The Kinetics of Formation of Anodic Tantalum Oxide — Further Studies," *J. Electrochem. Soc.*, 102, 655-659 (1955).

10. G. T. Burnstein and A. J. Davenport, "The Current-Time Relationship during Anodic Oxide Film Growth under High Electric Field," *J.*

Electrochem. Soc., 136, 936-941 (1989).

11. B. D. Cahan and C.-T. Chen, "The Nature of the Passive Film on Iron. III. The Chemi-Conductor Model and Further Supporting Evidence," *J. Electrochem. Soc.*, 129, 921-925 (1982).

12. C. P. Bean, J. C. Fisher, and D. A. Vermilyea, "Ionic Conductivity of Tantalum Oxide at Very High Fields," *Physical Review*, 101, 2, 551-554 (1956).

13. L. L. Odynets, "Ionic Transport in Anodic Oxide Films in Strong Fields," *Elektrokhimiya*, 26, 1040-1043 (1990).

14. J. F. Dewald, "The Effects of Space Charge on the Rate of Formation of Anode Films," *Acta Met.*, 2, 340-341 (1954).

15. J. F. Dewald, "A Theory of the Kinetics of Formation of Anode Films at High Fields," *J. Electrochem. Soc.*, 102, 1-6 (1955).

16. M. J. Dignam, "Transition Layer Model of the Oxide-Electrolyte Interface," *Can. J. Chem.*, 56, 595-605 (1978).

17. C. J. Greyling, I. A. Kotze, and P. E. Viljoen, "The Kinetics of Oxide Film Growth on Maraging Steel as Described by Space-charge Effects," *Surf. Interface Anal.*, 16, 293-298 (1990).

18. N. Sato and M. Cohen, "The Kinetics of Anodic Oxidation of Iron in Neutral Solution," *J. Electrochem. Soc.*, 111, 512-522 (1964).

19. B. E. Conway, B. Barnett, H. Angerstein-Kozlowska, and B. V. Tilak, "A Surface-Electrochemical Basis for the Direct Logarithmic

Growth Law for the Initial Stages of Extension of Anodic Oxide Films Formed at Noble Metals," *J. Chem. Phys.*, **93**, 8361-8373 (1990).

20. J. Frenkel, "Über die Warmebewegung in festen und flüssigen Körpern," *Z. f. Physik*, **35**, 652-669 (1926).

21. D. D. Macdonald and M. Urquidi-Macdonald, "Theory of Steady-State Passive Films," *J. Electrochem. Soc.*, **137**, 2395-2402 (1990).

22. D. D. Macdonald, S. R. Biaggio, and H. Song, "Steady-State Passive Films. Interfacial Kinetic Effects and Diagnostic Criteria," *J. Electrochem. Soc.*, **139**, 170-177 (1992).

23. B. MacDougall, "Role of Oxide Defects in the Anodic Oxidation of Nickel," *J. Electrochem. Soc.*, **127**, 789-795 (1980).

24. B. MacDougall, "Interpretation of Log*i* - Log*t* Relationships for Nickel Passivation," *J. Electrochem. Soc.*, **130**, 114-117 (1983).

25. G. Dagan and M. Tomkiewicz, "Passivation of Permalloy Thin Films. I. Kinetics of Anodic Oxidation in Neutral Solutions," *J. Electrochem. Soc.*, **139**, 461-466 (1992).

26. C. Lukac, J. B. Lumsden, S. Smialowska, and R. W. Staehle, "Effects of Temperature on the Kinetics of Passive Film Growth on Iron," *J. Electrochem. Soc.*, **122**, 1571-1579 (1975).

27. P. Russell and J. Newman, "Anodic Dissolution of Iron in Acidic Sulfate Electrolytes. I. Formation and Growth of a Porous Salt Film," *J. Electrochem. Soc.*, **133**, 59-69 (1986).

28. C. Wagner, "The Electrochemistry of Ionic Crystals," *J. Electrochem. Soc.*, 99, 346C-354C (1952).

29. P. G. Shewmon, *Diffusion in Solids*, McGraw-Hill, New York (1963).

30. O. T. Sørensen, *Nonstoichiometric Oxides*, Academic Press, Inc., New York, New York (1981).

31. J. Newman, *Electrochemical Systems*, 2nd Edition, Prentice-Hall Inc., Englewoods Cliffs, NJ (1991).

32. Y.- T. Chin and B. D. Cahan, "An Ellipsometric Spectroscopic Study of the Passive Film on Iron-Potential and Chloride Ion Dependence," *J. Electrochem. Soc.*, 139, 2432-2442 (1992).

33. M. Hänisch and A. Otto, "Differential Reflection Spectroscopy of Passive Films on Iron," *J. of Electroanalytical Chem. and Inter. Electrochem.*," 308, 113-126 (1991).

34. J. Gui and T. M. Devine "Obtaining Surface-Enhanced Raman Spectra from the Passive Film on Iron," *J. Electrochem. Soc.*, 138, 1376-1384 (1991).

35. M. Kerkar, J. Robinson, and A. J. Forty, "In-Situ Structural Studies of the Passive Film on Iron and Iron/Chromium Alloys using X-Ray Absorption Spectroscopy," *Faraday. Dis. of the Chem. Soc.*, 89, 31-40 (1990).

36. C. Wagner, "Models for Lattice Defects in Oxide Layers on Passivated Iron and Nickel," *Ber. Bunsenges. Phys. Chem.*, 77, 1090-1097

(1973).

37. V. Jovancicevic, R. C. Kainthla, Z. Tang, B. Yang, and J. O'M. Bockris, "The Passive Film on Iron: An Ellipsometric-Spectroscopic Study," *Langmuir*, 3, 388-395 (1987).

38. M. Pourbaix, *Atlas of Electrochemical Equilibria in Aqueous Solutions*," National Association of Corrosion Engineers, Houston, Texas, 313-317 (1974).

39. U. F. Franck and K. G. Weil, "Zur Korrosion despassiven Eisens in Schwefelsäure," *Z. f. Elecktrochemie*, 56 814-822 (1952).

40. R. C. Weast, *CRC Handbook of Chemistry and Physics*, Edition 59, CRC Press, Inc., Boca Raton, Florida (1978-1979).

41. W. Schmickler and J. W. Schultze, "Electron Transfer Reactions on Oxide-Covered Metal Electrodes," *Modern Aspects pf Electrochemistry*, Edited by J. O'M. Bockris, B. E. Conway, and R. E. White, Plenum Press, New York, 17, 357-410 (1986).

42. C. G. Hill, Jr., *An Introduction to Chemical Engineering Kinetics & Reactor Design*, John Wiley & Sons, Inc., New York (1977).

LAWRENCE BERKELEY LABORATORY
UNIVERSITY OF CALIFORNIA
TECHNICAL INFORMATION DEPARTMENT
BERKELEY, CALIFORNIA 94720